Clay Minerals, (2016) **51**, 197–211

Effect of layer charge on the crystalline swelling of Na^+, K^+ and Ca^{2+} montmorillonites: DFT and molecular dynamics studies

ANNIINA SEPPÄLÄ[1,*], EINI PUHAKKA[2] AND MARKUS OLIN[1]

[1] *VTT Technical Research Centre of Finland Ltd, P.O. Box 1000, FI-02044 VTT, Finland*
[2] *Laboratory of Radiochemistry, Department of Chemistry, P.O. Box 55, FI-00014 University of Helsinki, Finland*

(*Received 31 May 2015; revised 4 March 2016; Guest editor: Reiner Dohrmann*)

ABSTRACT: The swelling and cation exchange properties of montmorillonite are fundamental in a wide range of applications ranging from nanocomposites to catalytic cracking of hydrocarbons. The swelling results from several factors and, though widely studied, information on the effects of a single factor at a time is lacking. In this study, density functional theory (DFT) calculations were used to obtain atomic-level information on the swelling of montmorillonite. Molecular dynamics (MD) was used to investigate the swelling properties of montmorillonites with different layer charges and interlayer cationic compositions. Molecular dynamics calculations, with CLAYFF force field, consider three layer charges (–1.0, –0.66 and –0.5 e per unit cell) arising from octahedral substitutions and interlayer counterions of Na, K and Ca. The swelling curves obtained showed that smaller layer charge results in greater swelling but the type of the interlayer cation also has an effect. The DFT calculations were also seen to predict larger *d* values than MD. The formation of 1, 2 and 3 water molecular layers in the interlayer spaces was observed. Finally, the data from MD calculations were used to predict the self-diffusion coefficients of interlayer water and cations in different montmorillonites and in general the coefficient increased with increasing water content and with decreasing layer charge.

KEYWORDS: molecular dynamics, density functional theory, layer charge, montmorillonite, swelling, diffusion.

Smectites are 2:1 layered swelling clay minerals consisting of layers formed of two tetrahedral silicate sheets one on either side of an octahedral aluminium sheet. The charged layers have a negative charge and are stacked together with an interlayer space containing hydrated charge-compensating cations. Smectites have the ability to adsorb water in the interlayer space and to modify the cationic composition (Brigatti *et al.,* 2006; Velde & Meunier, 2008).

The properties of smectites are under extensive study due to their important role in a wide variety of technological and biochemical applications such as fluid filtration, catalytic processes and the disposal of high-level radioactive waste (Murray, 2000; Dohrmann *et al.,* 2013). In the Finnish concept of geological disposal of nuclear waste, a multi-barrier system is planned to prevent/retard the release of radionuclides to the biosphere. One of these barrier materials is bentonite which consists largely of the smectite-group mineral, montmorillonite. The retardation of radionuclides is based mainly on diffusional transport and sorption on solid mineral surfaces. Due to the presence of smectites, bentonite swells in contact with water thus blocking transport pathways.

Montmorillonite is a fine-grained and mechanically stable mineral characterized by layer charge (e/unit cell)

*E-mail: Anniina.Seppala@vtt.fi
DOI: 10.1180/claymin.2016.051.2.07

with the distribution of charge sites between the octahedral and tetrahedral sheets. The swelling and cation exchange properties of the mineral also depend on solution properties such as pH, ionic strength and ligands.

Isotopic difference neutron diffraction and molecular modelling techniques have made it possible to study the interlayer structure of clay and the effect of hydration on the clay structure (Sposito *et al.,* 1999). In sorption studies, molecular modelling has typically been used with surface characterization techniques such as X-ray photoelectron spectroscopy (Ebina *et al.,* 1999) and extended X-ray absorption fine structure spectroscopy (Hattori *et al.,* 2009). The relationship between atomistic phenomena and surface complexation modelling has also been formulated by Wesolowski *et al.* (2009). Quantum mechanics (QM) techniques have been used to study clay–cation and clay–cation–water interactions (Chatterjee *et al.,* 1999; Sposito *et al.,* 1999; Ren *et al.,* 2012; Tribe *et al.,* 2012). A recent multiscale approach including *ab initio* molecular dynamics (MD), classical MD and mesoscopic simulations emphasized the challenge in describing the phenomena with different length and time scales in clay studies (Rotenberg *et al.,* 2014). The benefits of using molecular modelling are evident because the understanding of the chemical reactions requires that the description of the electron structure of the system and the dependence of the thermodynamics as a function of time are known.

MD is used to study larger and more complex systems as compared to QM, e.g. to evaluate equilibrium and transport properties that cannot be calculated analytically (Tambach *et al.,* 2004; Tao *et al.,* 2010). While these properties are determined in the microscopic *i.e.* atomistic level, they are linked to the macroscopic properties of the bulk system through thermodynamics and statistical mechanics. In this work, QM and MD simulations are used to study the effect of layer charge on the swelling properties of montmorillonite. Although the swelling of montmorillonite has been studied extensively using molecular modelling, the structures used in those studies vary in terms of the location of substitutions (tetrahedral and/or octahedral), the layer charges and the types of interlayer cations (all of which may affect the swelling properties). While considering the effect of layer charge on the crystalline swelling of montmorillonite, comparison of results from different sources increases the number of variables leading to uncertainty in the comparison. In the present study, the layer charge stems only from octahedral substitutions and the same structures are applied for different interlayer cations, rendering comparison of the results more reliable. In addition, two different molecular modelling methods (QM and MD) are applied to the same structures, making comparison of the methods straightforward. The QM simulations are performed for a tridimensional periodic system, and MD simulations for a rectangular simulation box containing one clay lamella and the interlayer filled with water and cations. The optimized mineral structures defined by the QM methods are utilized in MD simulations. The results from the small-scale system QM calculations are compared with those from the slightly larger-scale system MD calculations. For the MD simulations, the simulation box was large enough to describe specific chemical interactions in the system in order to compare between different types of montmorillonites. Using larger systems, bending of clay lamellae, for example, may prohibit the detection of nanoscale phenomena.

METHODS

Montmorillonite structure

The basic montmorillonite building unit is a 2:1 layer with an octahedral (O) sheet sandwiched between two tetrahedral (T) sheets (Viani *et al.,* 2002). The TOT layers have a characteristic repeat distance and carry a net negative charge. The general unit-cell formula for Mg-substituted montmorillonite where the substitutions, *i.e.* charged sites, occur only in the octahedral sheet is

$$Si_8\left(Al_{4-x}Mg_x\right)O_{20}(OH)_4M^{k+}_{x/k}\cdot nH_2O \qquad (1)$$

where M is an alkali or alkali earth exchangeable cation (Na^+, K^+ or Ca^2) and $x = 0.4–1.2$. Because the number of charge sites in the tetrahedral sheet is small compared to the number of sites in the octahedral sheet (Rowe *et al.,* 1997), tetrahedral substitutions were not included in our small-scale calculations. The structure has a $C2/m$ symmetry, and experimental lattice parameters are $a =$ 518 pm, $b = 897$ pm, $c = 995$ pm, $\alpha = \gamma = 90.0°$ and $\beta =$ 99.5° without water molecules in the interlayer space between the TOT layers.

Quantum mechanics

In order to perform reliable MD calculations, accurate crystal structures of pure montmorillonites are required as a starting point for the calculations. In the present study, the optimized unit-cell structures were determined from QM for Na-, K- and Ca-montmorillonites. As a starting point for QM calculations, experimental atomic coordinates defined by

Tsipursky and Drits (1984) for K-smectite were used. The calculations were performed with the density functional *CASTEP* (CAmbridge Serial Total Energy Package, Clark *et al.,* 2005) code implemented in the *Materials Studio* versions 6.0 (Accelrys, 2011) and 7.0 (Accelrys, 2013).

Optimization of the unit cell of K-montmorillonite was performed using different exchange-correlation energy potentials, pseudopotentials and kinetic cut-off energy values to validate the results compared to experimental values. The exchange-correlation was described with generalized gradient approximation GGA-PBE or GGA-PW91. In these calculations, the total electronic energy and overall electronic density distribution were solved in order to define the energetically stable montmorillonite structures (Leach, 2001). As a compromise between the accuracy and computational time of calculations, the ultrasoft pseudopotentials (Table 1) were used for each element, and the kinetic cut-off energy for a plane-wave expansion of the wave function was 310 eV.

Optimizations of the unit cells of Na- and Ca-montmorillonites were done using GGA-PBE approximation only. The pseudopotentials are presented in Table 1, and the kinetic cut-off energy for a plane-wave expansion of the wave function was 310 eV as in the case of K-montmorillonite.

The optimized unit cells were used to construct model structures (1 × 3 × 1 unit cells) for MD simulations. The model structures were reoptimized using GGA-PBE approximation with the pseudopotentials presented in Table 1. For oxygen and silicon, O_00PBE.usp and Si_00PBE.usp potentials were used. In these calculations, the kinetic cut-off energy for a plane-wave expansion of the wave function was 370 eV.

Table 1. Pseudopotentials used in QM calculations.

	GGA-PBE	GGA-PW91
Al	Al_00PBE.usp	Al_00PBE.usp
Ca	Ca_00PBE.usp	Ca_00PBE.usp
H	H_00PBE.usp	H_00PBE.usp
K	K_00PBE.usp	K_00PBE.usp
Mg	Mg_00.usp	Mg_00PW91.usp
Na	Na_00PBE.usp	Na_00PBE.usp
O	O_00PBE.usp O_soft00.usp	O_00PBE.usp
Si	Si_00PBE.usp Si_soft00.usp	Si_00PBE.usp

The 1 × 3 × 1 model structures were utilized to study enlargement of the montmorillonite structure as a function of water insertion into the interlayer space of montmorillonites. Optimization of the model structures with different water contents was performed using the GGA-PW91 approximation. GGA-PW91 gives better description of the system, and calculations achieve convergence faster than using GGA-PBE. Further, the GGA-PBE overestimates the thickness of the interlayer space for larger systems, because it cannot describe the energy states of the system correctly. Calculations were performed using the pseudopotentials presented in Table 1. The kinetic cut-off energy for a plane-wave expansion of the wave function was 370 eV.

Hydration of cations was investigated using the density functional DMol3 code implemented in *Materials Studio* version 7.0 (Accelrys, 2013). The coordination sphere of cations (Na^+, K^+ and Ca^{2+}) was optimized using the GGA-PW91 approximation with DNP basis set and DFT-based semi-core pseudopotentials. Hydration energies were calculated as a difference between the total energy of a hydrated cation and the total energies of a non-hydrated cation and water molecules.

Molecular dynamics

All of the MD simulations in the present work were conducted using the *LAMMPS* (Plimpton, 1995) simulation software. The interatomic interactions for these hydrated montmorillonite systems were simulated using the *CLAYFF* (Cygan *et al.,* 2004) force field which was chosen because of its previous successful use in montmorillonite mineral simulations (Greathouse & Cygan, 2005; Tao *et al.,* 2010). The *CLAYFF* model differentiates an element into different types based on its structural position (tetrahedral or octahedral sheet and the neighbouring elements, *e.g.* substitution sites) and assigns partial charges and van der Waals parameters to each atom type. It defines a bond-stretch parameter for the structural hydroxyl groups and an angle bend parameter for the octahedral metal and OH. The interlayer water parameters in *CLAYFF* are from the flexible simple point charge (SPC) water model (Berendsen *et al.,* 1981). Simulations were performed in the isothermal-isobaric (NPT) ensemble with three-dimensional periodic boundary conditions. After pre-equilibration the systems were equilibrated for 0.5 ns, followed by the production run for another 0.5 ns at a temperature of 298 K and at pressure of 1 bar . A time step of 1 fs was

used in the production run. To avoid translational drift of the clay layer, the centre of mass of the layer was fixed during the simulation. The data were recorded every 200 fs. The long-range electrostatic interactions were calculated using the Ewald summation method (Karasawa & Goddard, 1989) with a precision of 1e–4. The short-range electrostatic and van der Waals interactions were calculated using a 12.5 Å cut-off.

The initial montmorillonite structure for the simulations was obtained from QM calculations. Simulations were performed using three different layer charges for montmorillonite: –1.0 e/unit cell ($x = 1$, *i.e.* one substitution per unit cell named later as Al3Mg1), –0.66 e/unit cell ($x = 0.66$, *i.e.* two substitutions per three unit cells, referred to as Al10Mg2) and –0.5 e/unit cell ($x = 0.5$, *i.e.* one substitution per two unit cells, named as Al7Mg1). The rectangular MD simulation box contains one clay lamella and the interlayer with water and cations. The clay layer contains 4×4 unit cells measuring 20.7 Å × 35.8 Å (with layer charges of –1.0 and –0.5 e/unit cell) or 6×3 unit cells measuring 31.1 Å × 26.9 Å (with a layer charge of –0.66 e/unit cell). Skipper *et al.* (1995) studied the effect of simulation box size and shape on the calculated interlayer properties and validated the use of a rectangular box containing eight unit cells (measuring 21.12 Å × 18.28 Å × 6.54 Å) of clay mineral. In the present study, a decision was taken to use a larger cell size in the *xy* plane to ensure the presence of multiple cations in each system. A snapshot of a rectangular Ca-montmorillonite simulation box is shown in Figure 1. The water content ranged from 1 to 16 molecules per unit cell (~0.02–0.4 g of H_2O/g clay) in each case. These calculations considered only the equilibrium state of montmorillonite when water is forced into the interlayer. After the system is relaxed, the mean value of the basal thickness (thickness of the layer and the interlayer) was obtained during the production run. The density profiles of interlayer atomic species were then derived in order to characterize the interlayer structure. Furthermore, in order to consider diffusion coefficients for interlayer water, the mean squared displacement (MSD) was calculated for water oxygens and cation species

$$\langle \triangle r^2(t) \rangle = \langle \left| r(t + t_0) - r(t_0) \right|^2 \rangle \qquad (2)$$

averaging over all the atoms considered and all choices for the time origin, t_0, from the recorded data (every 200 fs). The diffusion coefficient (D) was obtained from Einstein's relation

$$D = \lim_{t \to \infty} \frac{\langle \triangle r^2(t) \rangle}{2d * t} \qquad (3)$$

where d is the dimensionality and t is time. As diffusion is limited perpendicular to the clay layer, the coefficients were obtained for diffusion parallel to the layer using the two-dimensional Einstein equation.

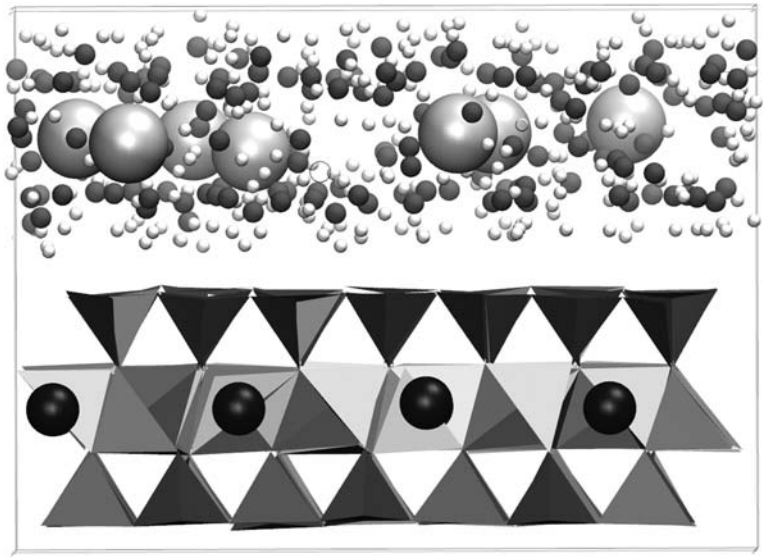

FIG. 1. A snapshot of the MD simulation box: Si (tetrahedra), Al (octahedra), Mg (black), O (dark grey), H (white) and Ca (light grey).

RESULTS AND DISCUSSION

Structures

The aim was to have comparable calculated and experimental lattice parameters of the unit-cell structures so that the modelling results could be utilized to interpret experimental findings. The lattice parameters from QM calculations for K-montmorillonite are presented in Table 2. The correspondence between the calculated and experimental parameters was satisfactory (Tsipursky & Drits, 1984; Bérend *et al.,* 1995). The calculations were performed with different approximations. The main difference between the approximations is how energy states of the system are described, especially partial densities originating from p-orbitals.

The Na- and Ca-montmorillonite structures were generated by replacing the K^+ ions with Na^+ ions to obtain Na-montmorillonite, and by replacing half of the K^+ ions with Ca^{2+} ions and removing the remaining half of K^+ ions to obtain Ca-montmorillonite. In this manner, the electrical neutrality of the structures was retained. The optimized structures and the optimized parameters are presented in Table 3.

In montmorillonites, the equivalent amount of exchangeable cations depends on the amount of Mg(II) atoms replacing Al(III) in the negatively charged octahedral sheets and the typical Mg:Al ratio is 1:5. In order to take into account the Mg:Al ratio in our studies and to retain the electrical neutrality of the models, the unit-cell structures had to be multiplied three times (1 × 3 × 1 unit cells in Fig. 2a). The positions of Mg

TABLE 2. Calculated lattice parameters for K-montmorillonite.

	Exptl[a]	GGA-PBE[b]	GGA-PBE[c]	GGA-PW91[d]
a (pm)	518	499.7	529.4	529.1
b (pm)	897	870.8	908.1	909.2
c (pm)	995	1 047.6	1 084.5	1 095.8
α (°)	90.0	90.0	90.0	90.0
β (°)	99.5	101.2	101.4	104.5
γ (°)	90.0	90.0	90.0	90.0
d value (pm)	981	1 027.6	1 063.0	1 060.9

[a]Tsipursky & Drits (1984).
[b]O_soft00.usp, Si_soft00.usp and Mg_00.usp.
[c]O_00PBE.usp, Si_00PBE.usp and Mg_00.usp.
[d]O_00PBE.usp, Si_00PBE.usp and Mg_00PW91.usp.

TABLE 3. Calculated lattice parameters for K-, Na- and Ca-montmorillonites: a unit cell (1 × 1 × 1) with 1:1 Mg:Al ratio (theoretical) and a threefold cell (1 × 3 × 1) with 1:5 Mg:Al ratio (real).

	K		Na		Ca	
	1 × 1 × 1	1 × 3 × 1	1 × 1 × 1	1 × 3 × 1	1 × 1 × 1	1 × 3 × 1
a (pm)	499.7	525.7	501.2	525.8	501.1	525.5
b (pm)	870.8	2 719.7	875.2	2 723.3	869.2	2 721.2
c (pm)	1 047.6	1 130 .0	1 161.3	1 087.5	1 023.8	1 049.2
α (°)	90.0	90.0	90.0	91.0	90.0	89.9
β (°)	101.2	100.7	114.2	97.2	108.1	100.9
γ (°)	90.0	90.0	90.0	90.0	90.0	90.0
d value (pm)	1 027.6	1 110.3	1 058.9	1 078.7	973.4	1 030.1

Note: no water present.

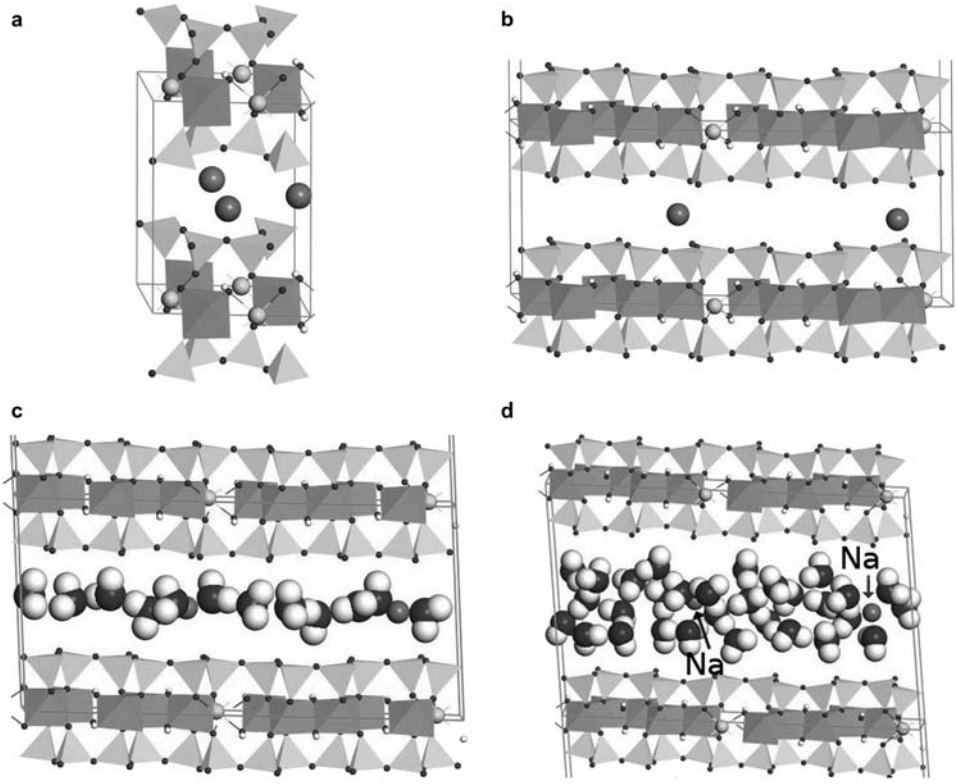

FIG. 2. (a) The unit cell of Na-montmorillonite from QM calculations; (b) the model structure (1 × 3 × 1 unit cells) for MD simulations, and Na-montmorillonite with (c) four and (d) ten water molecules per unit cell. Tetrahedral sheet: Si. Octahedral sheet: Al. Spheres in octahedral sheet: Mg. Small spheres in the octahedral and tetrahedral sheets: O. Interlayer: Na and water.

atoms were selected so the distance between them is as long as possible based on the symmetry. This selection agrees well with previous attempts (Lavikainen *et al.,* 2015). These new periodic models (Fig. 2b) were re-optimized and the optimized parameters for K-, Na- and Ca-montmorillonites are presented in Table 3.

Effect of water on the structures

Typically the so-called dry montmorillonite contains ~8–10 wt.% interlayer water. Based on the molecular mass of water and montmorillonite without interlayer water, the unit cell of the montmorillonite contains 2–4 water molecules. This means that, according to QM and MD simulations, only one water molecular layer exists in the interlayer space of the montmorillonite.

When the water content exceeded 10 wt.%, the interlayer space between the TOT layers began to increase, causing the swelling of the mineral. In this study, swelling was investigated with both QM and MD methods and QM was also used to detect possible atomic-level changes in the structure of the TOT layers.

In the QM calculations, the water content varied from 0 to 10 water molecules in the unit cell corresponding to 0–246 mg of H_2O/g of montmorillonite. Water molecules were added randomly into the interlayer space of the montmorillonite models one by one and the structure was re-optimized between each step. A corresponding technique was used in the earlier work based on Monte Carlo simulations (Zheng *et al.,* 2011). The Na-montmorillonite structure with 98.2 mg of H_2O/g of montmorillonite (~10 wt.%) is shown in Fig. 2c, and its lattice parameters are a = 525.7 pm, b = 2 714.1 pm, c = 1 324.1 pm, α = 93.2°, β = 96.4°, γ = 89.9°, and the d value is 1 313.9 pm. In comparison to the structure without water molecules the change of the lattice parameters is most remarkable in the c-axis direction increasing the distance (d value) between the TOT layers. The water molecules appear as molecules in the interlayer space, with no reactions with the TOT

layers. When ten water molecules were present in the unit cell of the montmorillonite, the water content was ~24 wt.%, and the swelling was ~33% in the *c*-axis direction (*d* value = 1747.6 pm) compared to the structure with 10 wt.% water. At least two molecular water layers exist between the TOT layers (Fig. 2d). More detailed analysis of the swelling results together with those obtained from MD calculations are presented later.

Hydration of cations

To understand the role of water in montmorillonite structures, the hydration of cations and clay layers has to be considered. Analysis of the coordination geometry of water molecules with cations reveals that free Na^+ has tetrahedral (Fig. 3a) or octahedral (Fig. 3b) coordination geometry with water molecules. K^+ also forms four- or six-coordinated complexes with water (Fig. 3c,d). The six-coordinated complex is trigonal prismatic. Free Ca^{2+} does not form four-coordinated complexes but occurs in octahedral form (Fig. 3e) or eight-coordinated square antiprismatic form (Fig. 3f). The hydration energies of Na^+, K^+ and Ca^{2+} cations are presented in Table 4. The coordination of the interlayer cations was analysed by Sposito *et al.* (1999) using Monte Carlo simulations.

In the interlayer space of montmorillonites, cations also tend to acquire corresponding coordination geometry like their free form in water solutions. The QM and MD simulations in the present study indicated that the interlayer water molecules form hydrogen bonds with the nearest cations and the oxygen atoms of the tetrahedral sheets. Na^+ typically has four water molecules in its coordination sphere, and further Na^+ can fulfil part of its coordination sites by forming van der Waals bonding with the oxygen atoms of the tetrahedral sheet. K^+ favours a six-coordinated complex with five water molecules and one van der Waals bond to the tetrahedral sheet. Ca^{2+} also favours a six-coordinated complex, so there are three coordinated water molecules and three van der Waals bonds to the tetrahedral sheet. Each of these structures varies case-by-case, however, depending on the orientation of the randomly set water molecules in the interlayer space.

Swelling of montmorillonites relates to the strength of interaction forces of water molecules with other water molecules, cations and tetrahedral sheets within the interlayer spaces. This expansion process is controlled by the balance of attractive *vs.* repulsive electrostatic forces resulting from the presence of negatively charged montmorillonite layers and interlayer cations. A variety of different intermolecular and electrostatic forces are valid, including hydrogen bonding, van der Waals forces, double layer repulsions and ion-ion correlation effects (Shirazi *et al.,* 2011).

Due to coulombic attractions between the negatively charged TOT layers and positively charged interlayer cations, the layers are initially held in close proximity to their neighbours. Van der Waals forces may also contribute to the total potential energy of attraction. The hydration energy of interlayer cations determines the total potential energy of repulsion, and thus the ease of penetration of water molecules into the interlayer space (Bérend *et al.,* 1995). These sites remain closed until the expansion pressure of the surrounding water phase overcomes the resistance to interlayer space opening. This allows for a single layer of water molecules to enter and reside within the interlayer space, which in turn leads to a reduction in the potential energy of attraction as neighbouring layers are separated by a greater distance.

Following this initial phase, the hydration of interlayer cations may begin. The extent of cation hydration and swelling of montmorillonites is largely determined by the type of interlayer cations and their hydration energies (Bérend *et al.,* 1995). In the case of the monovalent cations (Na^+, K^+) the degree of swelling is related to the hydration energy of the cations. However, hydration energies can vary significantly according to the degree of hydration of the cations (Table 4). Based on the greater hydration energies of the polyvalent cations (Ca^{2+}), the initial hydration occurs faster than for the monovalent cations, because Ca^{2+} as a polyvalent cation may take up more water molecules into its coordination sphere (up to eight water molecules) than Na^+ and K^+ as monovalent cations (Fig. 3). Hence, the hydrogen bonding of the Ca^{2+} cations with the tetrahedral sheet is stronger than that of the Na^+ and K^+ cations. In order to add extra water into the interlayer space, the free energy loss of the incoming water must be greater than the work done in increasing the interlayer space. Therefore, Na- and K-montmorillonites can take up more water than Ca-montmorillonite.

Swelling

The *d* spacing values of Na-, K- and Ca-montmorillonites with three different layer charges and varying interlayer water content were obtained from MD calculations where water was forced into the interlayer. The *d* values are given together with the QM results (using a layer charge of –0.66 e per unit cell), XRD results for Na-montmorillonite (Fu *et al.,* 1990),

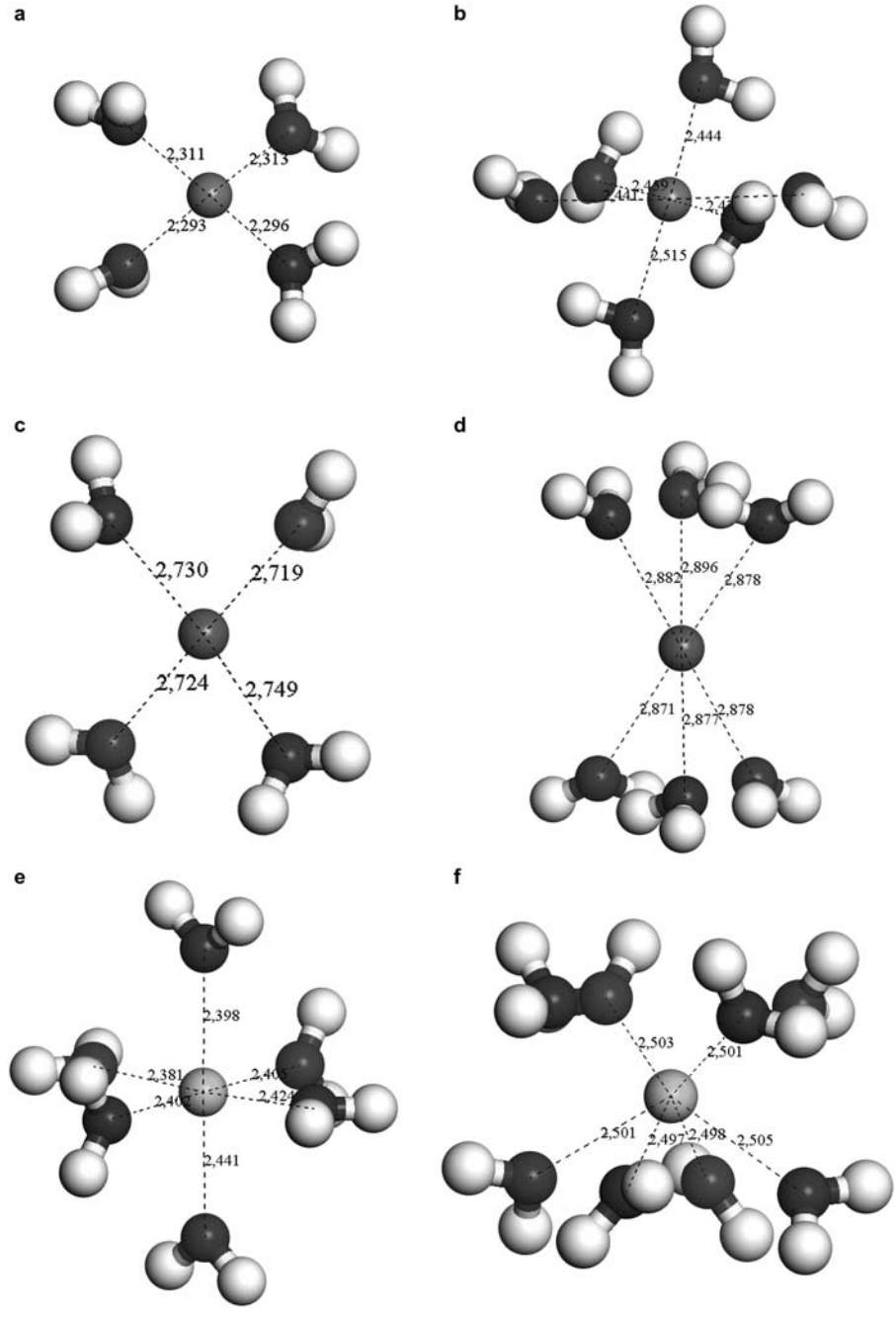

FIG. 3. Cation coordination in montmorillonites based on QM calculations: (a) four-coordinated Na^+; (b) six-coordinated Na^+; (c) four-coordinated K^+; (d) six-coordinated K^+; (e) six-coordinated Ca^{2+}; and (f) eight-coordinated Ca^{2+}.

for Ca-montmorillonite (Cases *et al.,* 1997) and for K-montmorillonite (Bérend *et al.,* 1995), and MC results from Zheng *et al.* (2011) for Na-montmorillonite with respect to the interlayer water content (Fig. 4). In each case, the MD results indicate that montmorillonites with smaller layer charges experience greater swelling.

TABLE 4. Hydration energies for Na^+, K^+ and Ca^{2+} cations.

	Hydration energy (kJ/mol)
$Na(H_2O)_4^+$	–397.73
$Na(H_2O)_6^+$	–534.24
$K(H_2O)_4^+$	–313.92
$K(H_2O)_6^+$	–458.81
$Ca(H_2O)_6^{2+}$	–1 123.96
$Ca(H_2O)_8^{2+}$	–1 294.24

In K-montmorillonite, however, the difference in swelling between the three structures is the smallest.

Comparison of the MD results for Na-, Ca- and K-montmorillonites with the same layer charges and water contents shows that, in general, K-montmorillonite exhibits the largest *d* value with the exception of Ca-montmorillonite for water contents of ~0.1–0.15 g/g_{clay}. This Ca result is consistent with the findings based on the hydration energies of different cations (Table 4) and is also supported by the XRD results. Denis *et al.* (1991) reported the influence of K in montmorillonite as a swelling inhibitor which is not observed in the present study because water is forced into the interlayer (note the absence of external water). The present QM results indicated that Na-montmorillonite exhibits the largest *d* value of >~0.2 g/g_{clay} of water content. Also, QM predicts larger *d* values than MD, but, in general, similarities can be detected (mainly for Ca-montmorillonite). The trends in the swelling graphs are generally in good agreement with the results from XRD and MC (for Na-montmorillonite). Differences in the experimental and simulation results may be due to the differences in the structures, like the presence of tetrahedral substitutions in the experimental samples.

Interlayer structures

Examples of density distributions of the interlayer water oxygens and cations for Na-, Ca- and K-montmorillonites

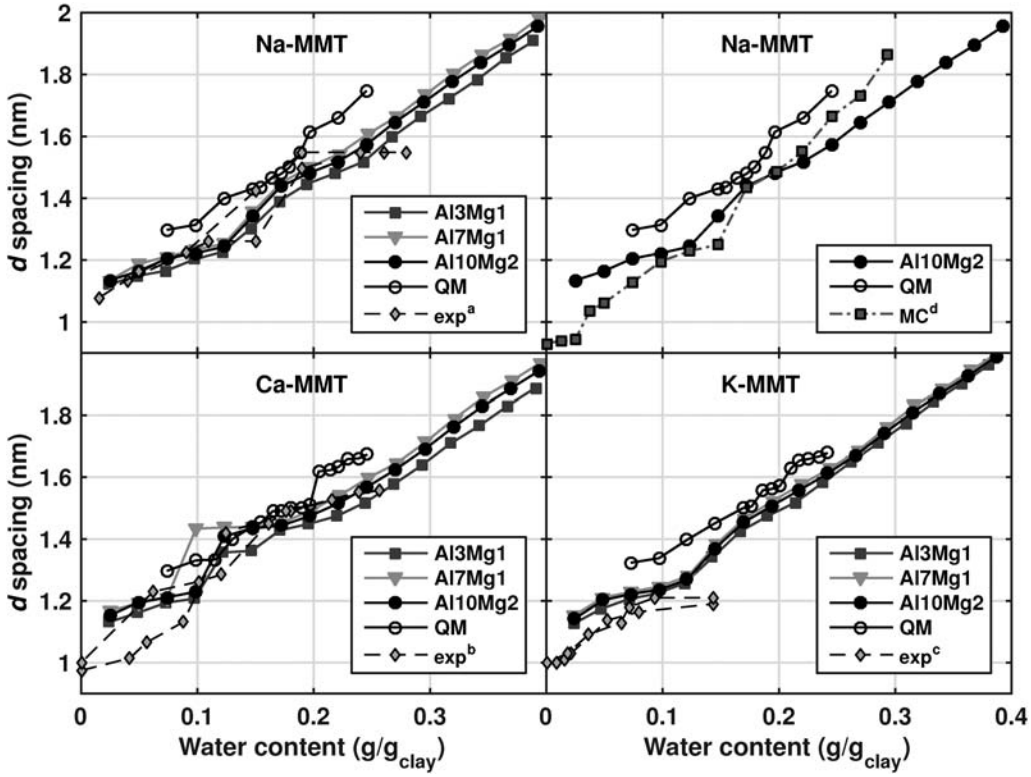

FIG. 4. The swelling curves of Na-, Ca- and K-montmorillonites with different layer charges from MD and QM studies (note: water is forced into the interlayer) and experimental results: (a) Fu *et al*. (1990), (b) Cases *et al*. (1997), (c) Bérend *et al*. (1995) and MC calculations from Zheng *et al*. (2011).

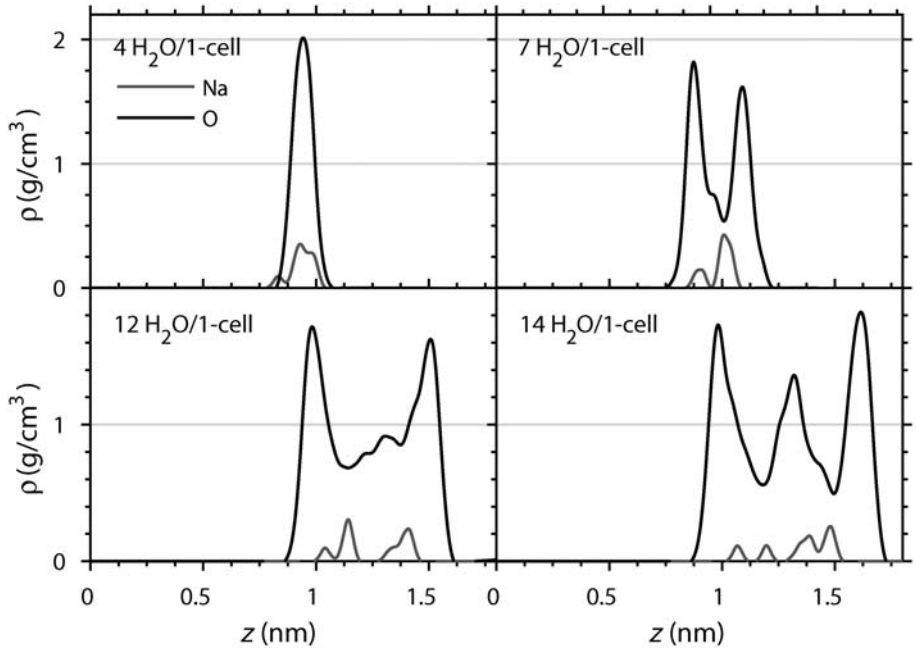

FIG. 5. Density distributions (from MD) of interlayer species for Na-montmorillonite (Al7Mg1) with interlayer water contents of 4, 7, 12 and 14 molecules/unit cell.

(layer charge 0.5 e per unit cell) are presented in Figures 5, 6 and 7, respectively. In these plots, the *x* axis is the basal distance from the bottom of the clay layer to the top of the interlayer space and the clay-layer thickness is ~0.64 nm (calculated from atom centre to atom centre). All density curves of water oxygens show peaks indicating the formation of water layers. For some water contents these peaks are not as distinct (*e.g.* Fig. 5 – bottom left hand corner). They are considered here as 'mixed states' when the previously existing water layers are 'full' and before the formation of yet another clearly separate layer is favoured. For Na-montmorillonite, the second water layer began to form when the water content increased to six molecules per unit cell and the third layer began to form at water contents of 10–11 molecules per unit cell. These regions are represented by a step in the swelling graphs in Fig 4. For Ca-montmorillonite, two water layers began to form when

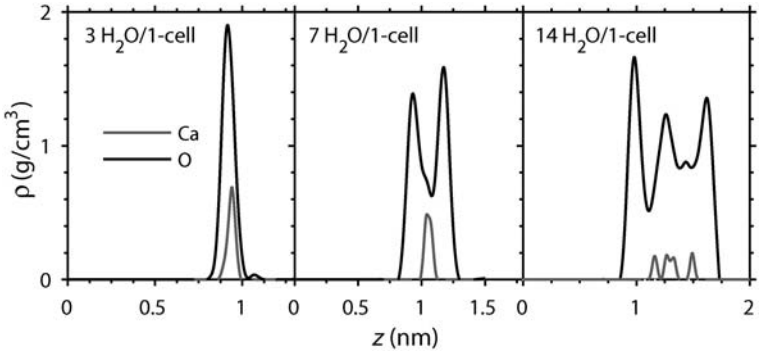

FIG. 6. Density distributions (from MD) of interlayer species (water oxygen and cation) for Ca-montmorillonite (Al7Mg1) with interlayer water contents of 3, 7 and 14 molecules/unit cell.

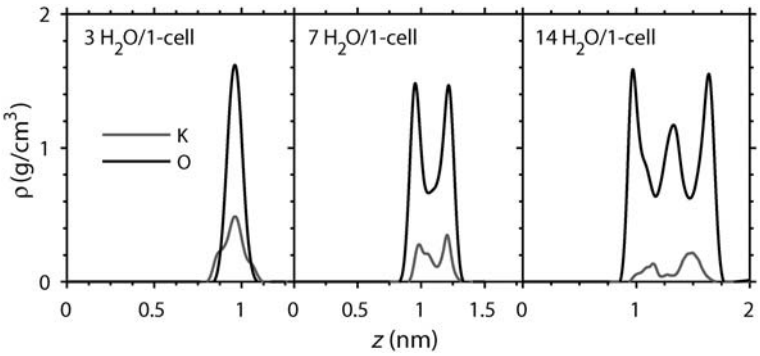

FIG. 7. Density distributions (from MD) of interlayer species (water oxygen and cation) for K-montmorillonite (Al7Mg1) with interlayer water contents of 3, 7 and 14 molecules/unit cell.

the water content increased to 4–5 molecules per unit cell and three water layers with 13–14 water molecules per unit cell. For K-montmorillonite, two water layers started to form when the water content increased to six molecules per unit cell and three water layers when the water was 12 water molecules per unit cell.

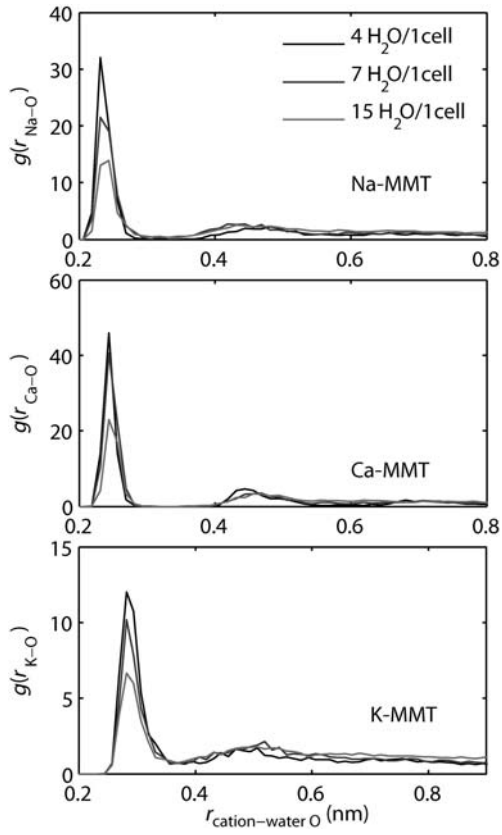

FIG. 8. RDF (from MD) for cation-water oxygen atoms for Na- and Ca-montmorillonites with layer charge of –0.5 e/unit cell and K-montmorillonite with layer charge of –1 e/unit cell.

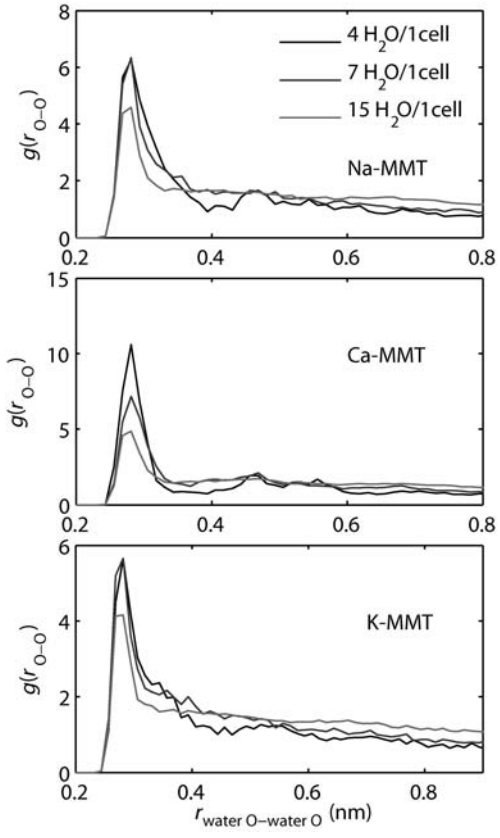

FIG. 9. RDF (from MD) for water O–water O atoms for Na- and Ca-montmorillonites with layer charge of –0.5 e/unit cell and K-montmorillonite with layer charge of –1 e/unit cell.

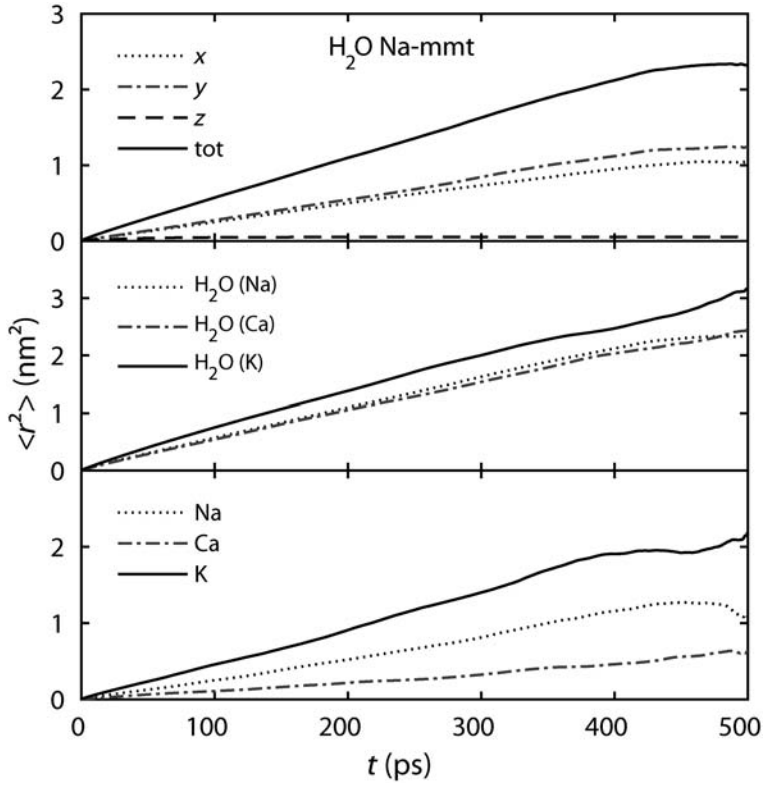

FIG. 10. MSD from MD calculations: *x, y, z* and total components for interlayer water in Na-montmorillonite with 10 H_2O/unit cell (top), interlayer water (O) in Na-, Ca and K-montmorillonites with 10 H_2O/unit cell (middle) and the interlayer cations (bottom).

The density distributions of Na in the plots indicate that the cations are surrounded by water molecules for most water contents, except at lower water contents (Fig. 5). The same behaviour was demonstrated by Ca-montmorillonite (Fig. 6). However, K cations are distributed more uniformly in the interlayer space indicating that they are not 'bound' between water layers (Fig. 7).

The radial distribution functions (RDF) of cation-water oxygens for one, two and three layer hydrates are presented in Fig. 8 for Na- and Ca-montmorillonites with layer charge of –0.5 e/unit cell and K-montmorillonite with layer charge of –1.0 e/unit cell. For Na-montmorillonite the first-neighbour peak was at ~0.23–0.24 nm in each hydrate case. For Ca-montmorillonite, this peak was at ~0.24–0.25 nm and for K-montmorillonite at ~0.28–0.29 nm in each case, in accordance with Tao *et al.* (2010). The RDFs of water oxygen-water oxygen for the corresponding cases are shown in Fig. 9. In each case the first-neighbour peak was at ~0.27–0.28 nm. However, the three-layer hydrate peak for Ca is shifted slightly when compared to the other two states.

Diffusion of water and cations

The MSDs of interlayer water (oxygens) and cations for Na-, Ca- and K-montmorillonites (Al10Mg2) with 10H_2O/unit cell as a function of time are shown in Fig. 10. According to Einstein's relation the slope of the MSD curve gives a quantitative measure of the diffusion coefficient. The statistics of the time correlation data deteriorate after half of the 500 ps run and especially for cations the statistics suffer from using a small number of particles (Fig. 10). To obtain the slope, a least-squares fit was done to 40–80% of the data up to 250 ps.

The values of the diffusion coefficients obtained for water and cations were presented together with the MD results from Holmboe & Bourg (2014),

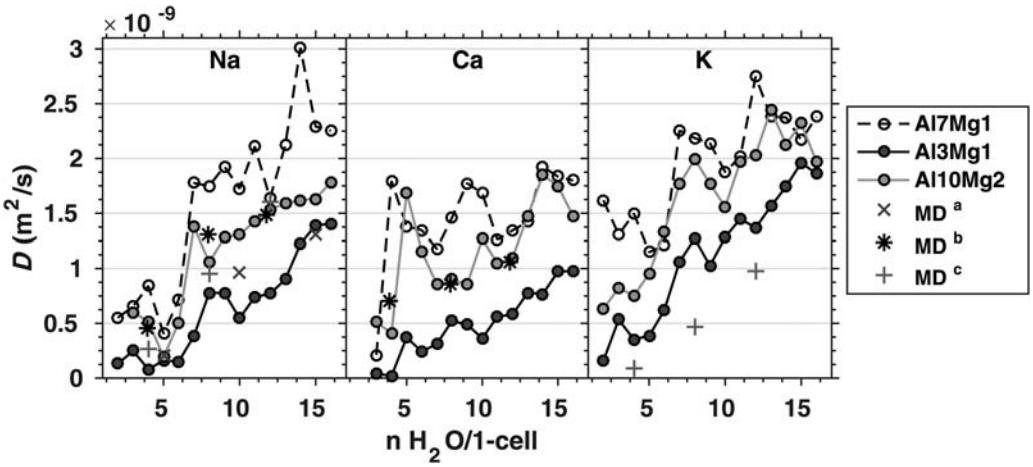

FIG. 11. The 2D interlayer water self-diffusion coefficients (from MD) for Na-, Ca- and K-montmorillonites and the MD results from: (a) Holmboe & Bourg (2014); (b) Greathouse *et al*. (2015); and (c) Boek (2014) (given in 3D).

Greathouse *et al.* (2015) and Boek (2014) (results reported for 3D diffusion and, thus, are lower than 2D values) in Figures 11 and 12, respectively. Note however, that calculation of the diffusion coefficients for cations suffers from use of small numbers of particles and, thus, only the values for montmorillonites with the larger layer charges (–0.66 and –1.0 e/unit cell) are reported. In general, the values increase with increasing water content and with decreasing layer charge. However, the increase was not linear. A rapid increase was observed in the values from monohydrate to bi-hydrate montmorillonite and, as the water content increased from approximately a half-saturated to a fully saturated hydrate structure, the diffusion coefficients decreased. In general, diffusion in Ca-montmorillonite is slower than in either the Na- or K-montmorillonites which is probably due to the different coordination and stronger interaction of the divalent Ca^{2+} *vs.* the monovalent Na^+ or K^+. The results are in satisfactory agreement with those from previous MD studies considering the different structures used.

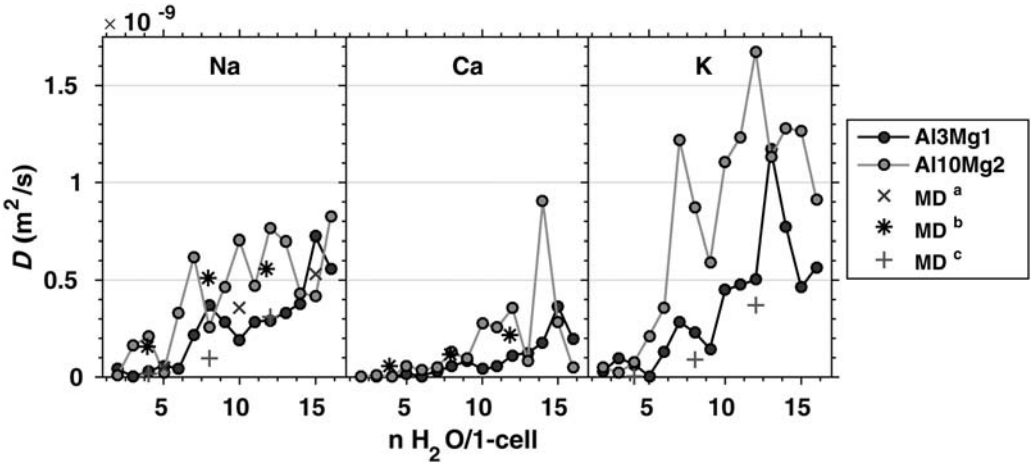

FIG. 12. The 2D interlayer cation self-diffusion coefficients (from MD) for Na-, Ca- and K-montmorillonites and the MD results from: (a) Holmboe & Bourg (2014); (b) Greathouse *et al*. (2015); and (c) Boek (2014) (given in 3D).

CONCLUSIONS

The present study indicated that both QM and MD can be used to study the crystalline swelling of montmorillonites. Based on the results for montmorillonites with only octahedral substitutions, smaller layer charge results in greater swelling, and the type of cation present in the interlayer also has a remarkable effect on the swelling properties. The MD simulations indicated that, in general, K-montmorillonite exhibits the largest *d* value, although the difference in the *d* value of different K-montmorillonites was minimal. The modelled swelling behaviour of K-montmorillonite contradicts the experimental observations where K acts as a swelling inhibitor. This is a result of the system setup. The simulations considered only the equilibrium state of a montmorillonite system where water is forced into the interlayer and the rate with which water is adsorbed was not taken into account. Similarities between the MD and QM results were detected, though in general QM predicts d values which are larger than those from MD. The likely reason reason is that QM calculations are static, and movement of atoms has not been taken into account as a function of time. Based on the MD calculations, the formation of water layers in the interlayer space of the montmorillonites, which is well known for natural samples, could be reproduced.

The data from MD calculations were also used to predict the self-diffusion coefficients of interlayer water and cations. The coefficient was not constant but increased non-linearly with increasing water content and with decreasing layer charge.

In the future, cation exchange reactions of montmorillonites in different salt concentrations should be studied in order to better describe the transport behaviour of water and cations in (and to) the interlayer space of montmorillonites. The hydration energies of cations in the interlayer space of montmorillonites and swelling pressures cannot be predicted based on these results, however.

The QM/MD techniques together are appropriate for studying the nanoscale interactions which determine macroscopic phenomena related to montmorillonites. In order to develop reliable continuum mechanics models, relevant nanoscale data are needed for input into these models.

ACKNOWLEDGEMENTS

The authors acknowledge the funding received from Posiva Oy.

NOMENCLATURE

CASTEP Cambridge serial total energy package
DNP Double Numerical plus Polarization
GGA-PBE Perdew, Burke and Ernzerhof version of generalized gradient approximation functional
GGA-PW91 Generalized gradient approximation (Perdew-Wang)
MD Molecular dynamics
O Octahedral
QM Quantum mechanics
T Tetrahedral

REFERENCES

Accelrys (2011) *MS Modeling, Release 6.0.* Accelrys Software Inc., San Diego

Accelrys (2013) *MS Modeling, Release 7.0.* Accelrys Software Inc., San Diego.

Bérend I., Cases J.M., Francois M., Uriot J.P., Michot L., Maison A. & Thomas F. (1995) Mechanism of adsorption and desorption of water vapor by homoionic montmorillonites: 2. The Li^+, Na^+, K^+, Rb^+ and Cs^+-exchanged forms. *Clays and Clay Minerals*, **43**, 324–336.

Berendsen H.J.C., Postma J.P.M., van Gunsteren W.F. & Hermans J. (1981) Interaction models for water in relation to protein hydration. Pp. 331–342 in: *Intermolecular Forces* (B. Pullman, editor). D. Reidel Publishing, Dordrecht, The Netherlands.

Boek E.S. (2014) Molecular dynamics simulations of interlayer and mobility in hydrated Li-, Na- and K-montmorillonite clays. *Molecular Physics*, **112**, 1472–1483.

Brigatti M.F., Galan E. & Theng B.K.G. (2006) Structures and mineralogy of clay minerals. Pp. 19–86 in: *Handbook of Clay Science*. Developments in Clay Science, **1**. Elsevier Ltd., Amsterdam.

Cases J.M., Bérend I., Francois M., Uriot J.P., Michot L.J. & Thomas F. (1997) Mechanism of adsorption and desorption of water vapor by homoionic montmorillonites: 2. The Mg^{2+}, Ca^{2+}, Sr^{2+} and Ba^{2+}-exchanged forms. *Clays and Clay Minerals*, **45**, 8–22.

Chatterjee A., Iwasaki T., Ebina T. & Miyamoto A. (1999) A DFT study on clay-cation-water interaction in montmorillonite and beidellite. *Computational Materials Science*, **14**, 119–124.

Clark S.J., Segall M.D., Pickard C.J., Hasnip P.J., Probert M.J., Refson K. & Payne M.C. (2005) First principles methods using CASTEP. *Zeitschrift fuer Kristallographie*, **220**, 567–570.

Cygan R.T., Liang J.-J. & Kalinichev A.G. (2004) Molecular models of hydroxide, oxyhydroxide, and

clay phases and the development of a general force field. *Journal of Physical Chemistry B*, **108**, 1255–1266.

Denis J.H., Keall M.J., Hall P.L. & Meeten G.H. (1991) Influence of potassium concentration on the swelling and compaction of mixed (Na, K) ion-exchanged montmorillonite. *Clay Minerals*, **26**, 255–268.

Dohrmann R., Kaufhold S. & Lundqvist B. (2013) The role of clays for safe storage of nuclear waste. Pp. 677–710 in: *Handbook of Clay Science, Techniques and Applications* (F. Bergaya and G. Lagaly, editors). Developments in Clay Science, Vol. **5B**, Elsevier, Amsterdam.

Ebina T., Iwasaki T., Onodera Y. & Chatterjee (1999) A comparative study of DFT and XPS with reference to the adsorption of caesium ions in smectites. *Computational Materials Science*, **14**, 254–260.

Fu M.H., Zhang Z.Z. & Low P.F. (1990) Changes in the properties of a montmorillonite-water system during the adsorption and desorption of water: hysteresis. *Clays and Clay Minerals*, **38**, 485–492.

Greathouse J.A. & Cygan R.T. (2005) Molecular dynamics simulation of uranyl(VI) adsorption equilibria onto an external montmorillonite surface. *Physical Chemistry Chemical Physics*, **7**, 3580–3586.

Greathouse J.A., Cygan R.T., Fredrich J.T. & Jerauld G.R. (2015) Molecular dynamics simulation of diffusion and electrical conductivity in montmorillonite interlayers. *The Journal of Physical Chemistry C*, **120**, 1640–1649.

Hattori T., Saito T., Ishida K., Scheinost A.C., Tsuneda T., Nagasaki S. & Tanaka S. (2009) The structure of monomeric and dimeric uranyl adsorption complexes on gibbsite: A combined DFT and EXAFS study. *Geochimica et Cosmochimica Acta*, **73**, 5975–5988.

Holmboe M. & Bourg I. (2014) Molecular dynamics simulations of water and sodium diffusion in smectite interlayer nanopores as a function of pore size and temperature. *The Journal of Physical Chemistry C*, **117**, 1001–1013.

Karasawa N. & Goddard W.A. (1989) Acceleration of convergence for lattice sums. *Journal of Physical Chemistry*, **93**, 7320–7327.

Lavikainen L.P., Tanskanen J.T., Schatz T., Kasa S. & Pakkanen T.A. (2015) Montmorillonite interlayer surface chemistry: effect of magnesium ion substitution on cation adsorption. *Theoretical Chemistry Accounts*, **134**, 2–7.

Leach A.R. (2001) *Molecular Modelling, Principles and Applications,* 2nd edition, Pearson Education Limited, Essex, UK.

Murray H.H. (2000) Traditional and new applications for kaolin, smectite, and palygorskite: a general overview. *Applied Clay Science*, **17**, 207–221.

Plimpton S.J. (1995) Fast parallel algorithms for short-range molecular dynamics. *Journal of Computational Physics*, **117**, 1–19.

Ren X., Yang S., Tan X., Chen C., Sheng G. & Wang X. (2012) Mutual effects of copper and phosphate on their interaction with γ-Al_2O_3: Combined batch macroscopic experiments with DFT calculations. *Journal of Hazardous Materials*, **237–238**, 199–208.

Rotenberg B., Marry V., Salanne M., Jardat M. & Turq P. (2014) Multiscale modelling of transport in clays from the molecular to the sample scale. *Comptes Rendus Geoscience*, **346**, 298–306.

Rowe R.K., Quigley R.M. & Booker, J.T. (1997) *Clayey Barrier Systems for Waste Disposal Facilities.* E & FN Spon, London.

Shirazi S.M., Wiwat S., Kazama H., Kuwano. & Shaaban M.G. (2011) Salinity effect on swelling characteristics of compacted bentonite. *Environment Protection Engineering*, **37**, 65–74.

Skipper N.T., Chang F.-R.C. & Sposito G. (1995) Monte Carlo simulations of the interlayer molecular structure in swelling clay minerals. 1. Methodology. *Clays and Clay Minerals,* **43,** 285–293.

Sposito G., Skipper N.T., Sutton R., Park S.-H., Soper A. K. & Greathouse J.A. (1999) Surface geochemistry of the clay minerals. *Proceedings of the National Academy of Sciences*, **96**, 3358–3364.

Tambach T.J., Hensen E.J.M. & Smit B. (2004) Molecular simulations of swelling clay minerals. *Journal of Physical Chemistry B*, **108**, 7586–7596.

Tao L., Xiao-Feng T., Yu Z. & Tao G. (2010) Swelling of K^+, Na^+ and Ca^{2+}–montmorillonites and hydration of interlayer cations: a molecular dynamics simulation. *Chinese Physics B,* **19,** 109101(1–7).

Tribe L., Hinrichs R. & Kubicki J.D. (2012) Adsorption of nitrate on kaolinite surfaces: A theoretical study. *The Journal of Physical Chemistry B*, **116**, 11266–11273.

Tsipursky S.I. & Drits V.A. (1984) The distribution of octahedral cations in the 2:1 layers of dioctahedral smectites studied by oblique-texture electron diffraction. *Clay Minerals*, **19**, 177–193.

Velde B. & Meunier A. (2008) *The Origin of Clay Minerals in Soils and Weathered Rocks.* Springer-Verlag, Berlin Heidelberg.

Viani A., Gualtieri A.F. & Artioli G. (2002) The nature of disorder in montmorillonite by simulation of X-ray powder patterns. *American Mineralogist*, **87**, 966–975.

Wesolowski D.J., Bandura A.V., Cummings P.T., Fenter P. A., Kubicki J.D., Lvov S.N. Machesky M.L., Mamontov E., Předota M., Ridley M.K., Rosenqvist J., Sofo J.O., Vlcek L. & Zhang Z. (2009) Atomistic origins of mineral-water interfacial phenomena and their relation to surface complexation models. *Geochimica et Cosmochimica Acta,* **73,** A1429.

Zheng Y., Zaoui A. & Shahrour (2011) A theoretical study of swelling and shrinking of hydrated Wyoming montmorillonite. *Applied Clay Science*, **51**, 177–181.